SCIENTIFIC REPORTS

OPEN

SUBJECT AREAS:
NANOTECHNOLOGY
CARBON NANOTUBES AND FULLERENES
THEORETICAL CHEMISTRY
CHEMICAL PHYSICS

Received
27 April 2012

Accepted
30 July 2012

Published
17 August 2012

Correspondence and requests for materials should be addressed to J.C.C. (jean-christophe.charlier@uclouvain.be), M.P. (panm@ornl.gov) or M.T. (mut11@psu.edu)

* These authors contributed equally to this work.

Nitrogen-doped graphene: beyond single substitution and enhanced molecular sensing

Ruitao Lv[1]*, Qing Li[2]*, Andrés R. Botello-Méndez[3]*, Takuya Hayashi[4], Bei Wang[1], Ayse Berkdemir[1], Qingzhen Hao[1], Ana Laura Elías[1], Rodolfo Cruz-Silva[4], Humberto R. Gutiérrez[1], Yoong Ahm Kim[4], Hiroyuki Muramatsu[4], Jun Zhu[1], Morinobu Endo[4], Humberto Terrones[1,5], Jean-Christophe Charlier[3], Minghu Pan[2] & Mauricio Terrones[1,4]

[1]Department of Physics, The Pennsylvania State University, University Park, PA 16802, USA, [2]Center for Nanophase Materials Sciences, Oak Ridge National Laboratory, Oak Ridge, TN 37831, USA, [3]Institute of Condensed Matter and Nanosciences, Université catholique de Louvain, Chemin des étoiles 8, 1348 Louvain-la-Neuve, Belgium, [4]Research Center for Exotic Nanocarbons, Shinshu University, Wakasato 4-17-1, Nagano-city 380-8553, Japan, [5]Physics Department, Ceará Federal University, Caixa Postal 6030 Fortaleza-Ceará, Brazil.

Graphene is a two-dimensional network in which sp^2-hybridized carbon atoms are arranged in two different triangular sub-lattices (A and B). By incorporating nitrogen atoms into graphene, its physico-chemical properties could be significantly altered depending on the doping configuration within the sub-lattices. Here, we describe the synthesis of large-area, highly-crystalline monolayer N-doped graphene (NG) sheets via atmospheric-pressure chemical vapor deposition, yielding a unique N-doping site composed of two quasi-adjacent substitutional nitrogen atoms within the same graphene sub-lattice (N_2^{AA}). Scanning tunneling microscopy and spectroscopy (STM and STS) of NG revealed the presence of localized states in the conduction band induced by N_2^{AA}-doping, which was confirmed by *ab initio* calculations. Furthermore, we demonstrated for the first time that NG could be used to efficiently probe organic molecules via a highly improved graphene enhanced Raman scattering.

Doping is an efficient way to tailor the electronic, chemical, optical and magnetic properties of materials[1–4], and this approach has been widely applied in semiconductor electronics and photovoltaic devices. Substitutional doping of graphene with different atoms (e.g. B, N, S and Si) results in the disruption of the ideal sp^2 hybridization of the carbon atoms, thus locally inducing significant changes in their electronic properties and chemical reactivity[5–9]. In particular, N-doping, expected to introduce additional *n*-type carriers in carbon systems, is crucial for applications in high-frequency semiconductor devices[6] and enhanced catalysis for energy conversion and storage[10–12]. In addition, N-doping could also enhance the biocompatibility of carbon nanomaterials[13,14] and therefore is favorable for biosensing applications[15]. Although some attention has been paid to the synthesis and potential applications of N-doped graphene (NG)[16–18], the atomic configurations of the N-dopants within the graphene sub-lattices have not been studied. Besides the doping concentration, the nature of the dopants, *e.g.* the bonding type, the dopant location and the induced perturbation within the graphene sub-lattices, are important to both basic research and practical applications. Zhao *et al.* prepared monolayer NG sheets using a low-pressure (high vacuum) chemical vapor deposition (LP-CVD) method and visualized the *single substitution* of carbon atoms by N-dopants (*i.e.* individual sp^2-like N-dopant, N_1) within the graphene lattice; this N_1 defect was notably abundant when studying all regions by scanning tunneling microscopy/spectroscopy (STM/STS)[19]. By using a solvothermal method, Deng *et al.* synthesized entangled multi-layer NG sheets and suggested a speculative model of *double substitution* (N_2)[20]. However, further theoretical and experimental works are still needed to elucidate diverse N-doping configurations within the graphene sheets and sub-lattices.

Here, we developed a simple but efficient method to synthesize large-area and highly-crystalline monolayer NG sheets on copper (Cu) foils by atmospheric-pressure chemical vapor deposition (AP-CVD). By performing STM/STS studies and *ab initio* simulations, we have demonstrated that as-synthesized NG sheets contain an abundant amount of N_2 dopants *within the same graphene sub-lattice* (N_2^{AA}) (e.g. ~80% dominance among all the identified defects), as well as other types of more complex configurations. It should be noted that the dominant

presence of the N_2^{AA} dopants is highly dependent on the experimental CVD setup and reaction parameters (see our control experiments in Supplementary Section S6). STS measurements confirmed by theoretical calculations reveal a spatial electronic localization close to the N-dopants in graphene. More interestingly, we have demonstrated for the first time that individual NG sheets could be used to efficiently identify organic molecules through a significant enhancement of the Raman signal, while pristine graphene sheets do not display such enhancement under the same Raman spectroscopy conditions. We therefore envision that NG sheets could provide a highly sensitive surface with controlled modifications for developing molecular nanosensors and *n*-type graphene-based electronic nanodevices.

Results

Large-area monolayer NG sheets were synthesized on Cu foils using methane (CH_4) and ammonia (NH_3) as precursors in an AP-CVD setup (for details see Methods, Supplementary Fig. S1 and Section S1). Figure 1a depicts a typical photograph of as-synthesized NG on Cu foil. Due to the high transparency of single graphene layers, the NG-covered Cu foil exhibits the intrinsic appearance of copper. In addition, the underneath Cu foil could be easily etched away in an aqueous $FeCl_3$/HCl solution (Fig. 1b). NG samples were then transferred onto other substrates (*e.g.* SiO_2/Si wafers) using a polymethyl methacrylate (PMMA)-assisted method[21] in order to keep large-area NG sheets from breaking during the transfer process. Figure 1c shows a transferred NG sheet with a 1 cm × 1 cm area. It is noteworthy that the size of the NG sample could be much larger and it only depends on the size of original Cu foil used for the transfer. High-resolution transmission electron microscopy (HRTEM) studies were performed after transferring as-synthesized NG onto TEM grids by a PMMA-free method[22] (see Supplementary Fig. S2, S3 and Section S2). Typical HRTEM images of NG sheets are shown in Figs.1d-e. The corresponding fast Fourier transform (FFT) of Fig. 1e reveals the hexagonal feature of the single-layer NG lattice. Occasionally, bi-layer and tri-layer islands could also be detected in NG samples by HRTEM. Both of them display distinct Moiré patterns caused by the stacking of individual hexagonal NG layers with different orientations (see Supplementary Fig. S4).

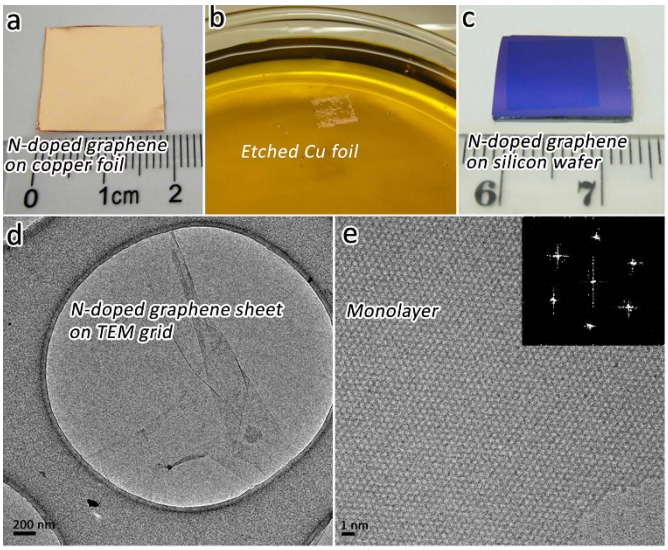

Figure 1 | Morphology of as-synthesized N-doped graphene (NG) sheets. (a) Photograph of as-synthesized NG sample on Cu foil. (b) PMMA-coated NG with Cu residues floating on $FeCl_3$/HCl aqueous solution, which is used as Cu etchant. Cu foil can be completely etched away within ~20 min. (c) NG sheet (1cm×1cm) on silicon wafer with 300 nm-thick SiO_2 coating. This NG sheet was only part of the prepared NG sample shown in (a). It could be any size depending on the dimension of original NG-covered Cu foil for transfer. (d-e) Typical HRTEM images of as-synthesized monolayer NG. The inset of (e) is the corresponding fast Fourier transform (FFT) depicting the hexagonal pattern characteristic of the graphene framework.

Representative Raman spectra of N-doped and pristine graphene on SiO_2/Si substrates using 514 nm laser excitation are shown in Fig. 2a. Both kinds of samples were synthesized under the same experimental conditions except for the introduction of NH_3 used for the N-doping. The symmetric line-shape of the 2D-band and the large ratio of the 2D-band over G-band intensities ($I_{2D}/I_G > 2$) confirm the growth of mostly a single layer in both NG and pristine graphene samples[23]. The D-band of pristine CVD graphene is presumed to be related to domain boundaries and growth nucleation sites[24]. The relatively weak D-band in pristine graphene sheets ($I_D/I_G \sim 0.12$) demonstrates a high degree of crystallinity for the undoped monolayers. In contrast, the NG spectra reveal a more intense D-band ($I_D/I_G \sim 1.00$), which can be explained by the elastically scattered photo-excited electron created by the large number of nitrogen atoms embedded in the graphene lattice before emitting a phonon. The average distance between defects (L_D) is roughly estimated to be *ca.* 10 nm and the defect density is *ca.* 1.2×10^{12} cm^{-2} from the ratio $I_D/I_G \sim 1.00$ of the NG sheets[25,26]. The Raman spectra of the NG also exhibit an obvious D'-band, which is believed to be originated from intravalley double resonance scattering processes[27]. Similar features have also been reported in NG sheets synthesized by LP-CVD[18,19,28]. Compared to that of pristine graphene, the Raman spectrum of NG shows a downshift of the G-band (2 cm^{-1}) and 2D-band (7 cm^{-1}). Based on the empirical relationship between the Fermi energy and the Raman peak position[29], the downshifts suggest that the N dopants move the Fermi level of graphene up by ~350 meV.

In order to further investigate the homogeneity of NG sheets, Raman mappings were acquired on a 50 μm × 50 μm area (see Fig. 2b and Supplementary Fig. S5a–c). Most of the scrutinized area within the NG sheet exhibits $I_{2D}/I_G > 2$, except for a few islands showing $I_{2D}/I_G \leq 1$ (see Fig. 2b), which correspond to the occasional presence of few-layer NG sheets, also witnessed by HRTEM (see Supplementary Fig. S4) and atomic force microscopy (AFM) (see Supplementary Fig. S5d). Based on HRTEM, AFM and Raman mappings, we concluded that as-synthesized NG samples are mostly homogeneous monolayer sheets.

The presence of nitrogen atoms in NG was further confirmed by X-ray photoelectron spectroscopy (XPS). For pristine graphene, the C1s line scan spectrum (Fig. 2c) exhibits a peak located at 284.6 eV, corresponding to the graphite-like sp^2 hybridized carbon. This peak is also dominant in NG, suggesting that most of the carbon atoms remain embedded within the honeycomb lattice. In addition, for the NG sample, we found two extra peaks located at ~285.8 and 288.2 eV, which could be attributed to C-N bonding and oxygenated groups structures[16]. It is important to emphasize that no signal could be detected in the N1s line scans from the pristine graphene samples. For the NG sheets, two signals were identified in the N1s line scans (shown in Fig. 2d), suggesting the presence of at least two types of N-C bonding: substitutional N located at 400.6 eV and a weak pyridine-like N signal located at 398.6 eV[30].

STM/STS measurements were performed after transferring NG sheets onto SiO_2/Si substrates (see Methods) because the Cu foil could affect STM imaging due to the charge screening in the graphene layer[31,32]. A large-area scan shows a rough surface with corrugations of 0.6~1.0 nm, which could be attributed to the roughness of the SiO_2/Si substrate. A representative STM topographic image of NG reveals the clear honeycomb lattice mostly decorated with brighter "*peapod-like graphic protrusions*", as pointed by white arrows in Fig. 3a. Since similar features were observed all over the NG surface and were never detected in pristine graphene, we propose

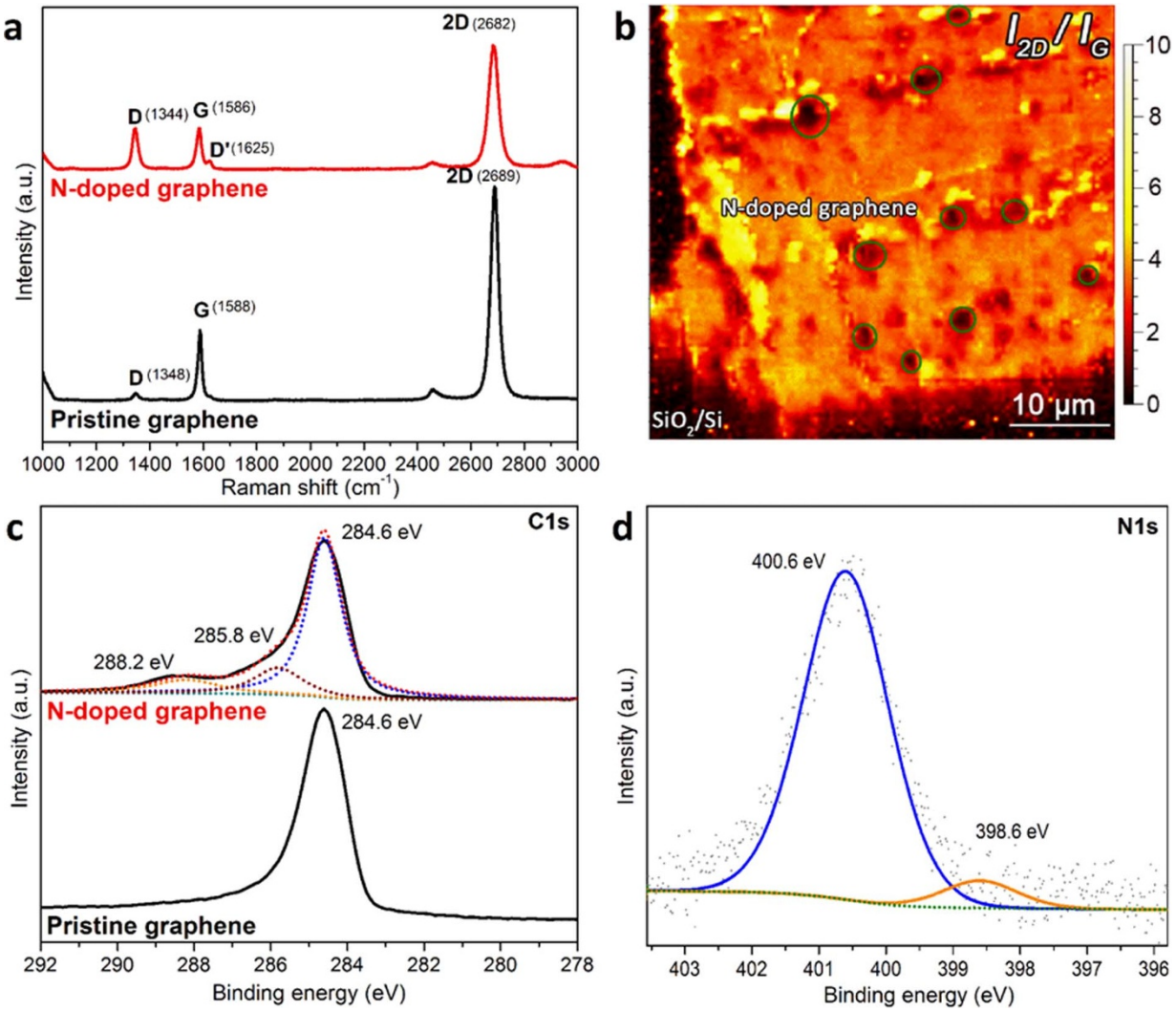

Figure 2 | Raman spectroscopy and X-ray photoelectron spectroscopy (XPS) characterizations of as-synthesized NG and pristine graphene samples. (a) Typical Raman spectra of N-doped and pristine graphene on SiO_2/Si substrate. The wavelength of Raman laser line is 514 nm. (b) 2D-band to G-band intensity ratio (I_{2D}/I_G) mapping of NG on SiO_2/Si substrate. The NG sample is composed of a majority of single-layer sheets and some bi-layer or tri-layer islands, as highlighted with dark circles in the image. (c) XPS C1s line scan of N-doped and pristine graphene. The main peak at 284.6 eV corresponds to the graphite-like sp^2 C, indicating most of the carbon atoms are arranged in honeycomb lattice. The small peaks at 285.8 and 288.2 eV can be attributed to C-N bonding and oxygenated groups structures. (d) N1s line scan of NG sample, which confirms the presence of substitutional (400.6 eV) and pyridine-like (398.6 eV) nitrogen dopants. The dashed green line exhibits the Shirley background.

that these specific features are caused by the presence of N-dopants. The FFT presented in Fig. 3a indicates the typical reciprocal hexagonal symmetry of the graphene lattice (outer hexagon) and inter-valley scattering peaks (inner hexagon), representing the enhanced electron scattering induced by N-dopants[33,34].

The highly-resolved STM image (Fig. 3b) provides a close-up topography of an individual N-doped site. The peapod-like feature is composed of a series of bright protrusions spaced *ca.* 2.4 Å, a value consistent with the second neighbor C-C spacing in the graphene lattice. It is worth noting that the topography of this type of N-doping site is different from previous reports[19], thus suggesting the presence of new bonding configurations for N-dopants. In order to elucidate these new doping configurations observed experimentally, density functional theory (DFT)-based STM simulations using the Tersoff-Hamann approach[35–37] within the generalized gradient approximation (GGA) for exchange and correlation[38] have been carried out. The calculated STM image (see Fig. 3c) displays a mirror plane passing through the carbon atom that has two nitrogen nearest neighbors (depicted as blue balls in the superposed ball-stick model), and four bright spots perpendicular to the mirror plane that are centered at the carbon atoms surrounding the N atoms. Visible features from the N-doped site observed by STM, and the overall triangular shape and mirror plane of the calculated STM images are in excellent agreement with experimental results. In particular, we confirmed the presence of almost two quasi-adjacent nitrogen atoms in substitution within the NG sheets. To our surprise, these two nitrogen atoms are separated by one carbon and sit consequently on the same A-sub-lattice, thus forming an N_2^{AA} configuration (see Supplementary Fig. S6).

Discussion

The *ab initio* computed formation energies for different types of N-doped graphene (Fig. 4a) confirm the stability of nitrogen atoms in substitution. As pointed out by our calculations, nitrogen atoms could also stabilize structural defects such as vacancies. Several simulated STM images are illustrated in Figs. 4b–e. We believe that the abundance of N_2^{AA} and the presence of other complicated configuration arise from our unique AP-CVD growth, which is operating at

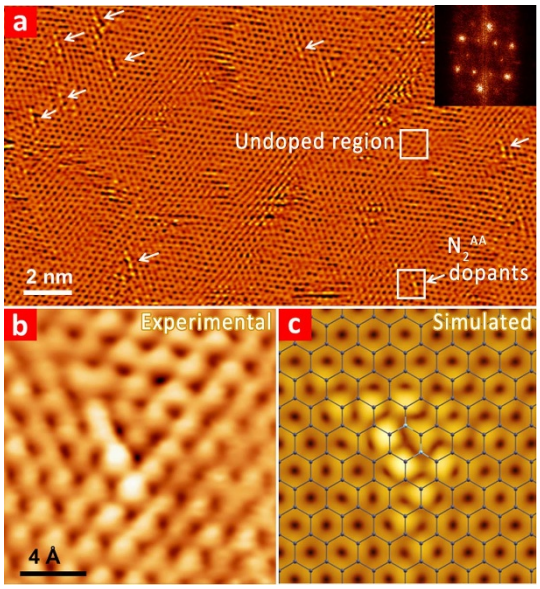

Figure 3 | Experimental and simulated STM images of as-synthesized NG sheets. (a) Large-area STM image of the NG illustrating the presence of numerous N-dopants with similar peapod-like configuration (highlighted by white arrows), V_{bias} = −75 mV, I_{set} = 100 pA. The upper and lower squares are used to indicate the undoped region and N_2^{AA} dopants. (Inset) FFT of topography presents reciprocal lattice (outer hexagon) and intervalley scattering (inner hexagon). The STM image shown here is obtained in flattening mode to remove the overall roughness of the substrate and enhance the atomic contrast of dopants. (b) Highly resolved STM image of a N_2^{AA} dopant. (c) Ball-stick structural model of the N_2^{AA} dopant and simulated STM image obtained using first-principles calculations. The bias is −1.0 eV. The carbon and nitrogen atoms are illustrated using gray and cyan balls, respectively.

ambient pressure, in contrast to the commonly used high-vacuum CVD reported for synthesizing NG[18,19,28]. The relatively high partial pressure of NH_3 molecules would lead to shorter mean free paths, thus enhancing intermolecular collisions and generating more doping defects within the graphene lattice. In addition, our STM observations indicate that most of the nitrogen incorporation occurs in the same sub-lattice (N_2^{AA}), as opposed to the other sub-lattice (N_2^{BB}) (see Supplementary Fig. S6). Indeed, among different doping configurations, we observed that more than 80% of the doping sites belong to the N_2^{AA} type. Some other less common doping defects found in our NG samples are shown in Fig. S7. Regarding the selective sub-lattice nitrogen doping mechanism, our total energy calculations indicate that it is energetically more favorable to introduce a second N_2^{AA} defect in the same A sub-lattice than to place it on the B sub-lattice (for details, see Fig. S8). Control experiments have been carried out by changing doping parameters in order to verify the effect of different NH_3 reaction temperatures and times, but keeping the CH_4 reaction temperature and time unchanged (980°C for 30 min). The Raman characterization analysis suggests that there is a competition between the incorporation of nitrogen atoms embedded within the graphene sheet and the annealing process in the presence of NH_3. This is observed after modifying both the reaction temperature (Fig.S9) and the reaction time (Fig.S10–S11). It can be seen that the I_D/I_G ratio, the G-band and the 2D-band change considerably. In particular, the D'-band does not show up in some cases. All of these variations reveal clear differences of nitrogen doping levels. We noted that only within a narrow window of NH_3 reaction time and temperature during the NG synthesis, the abundance of N_2^{AA} dopants occur. At lower temperatures (e.g. 750°C) and shorter reaction times (e.g. 5 min), it is more difficult for nitrogen atoms to incorporate into the graphene lattice (see Fig. S9–S10). At very high temperatures (e.g. 950°C, close to the graphene formation temperature), the graphene growth is inhibited by the reaction of carbon with gaseous NH_3, and thus no graphene sheets are formed (see Fig. S9). However, at very long NH_3 reaction times (e.g. 60 min), we observed that the NG sample becomes more crystalline and defect

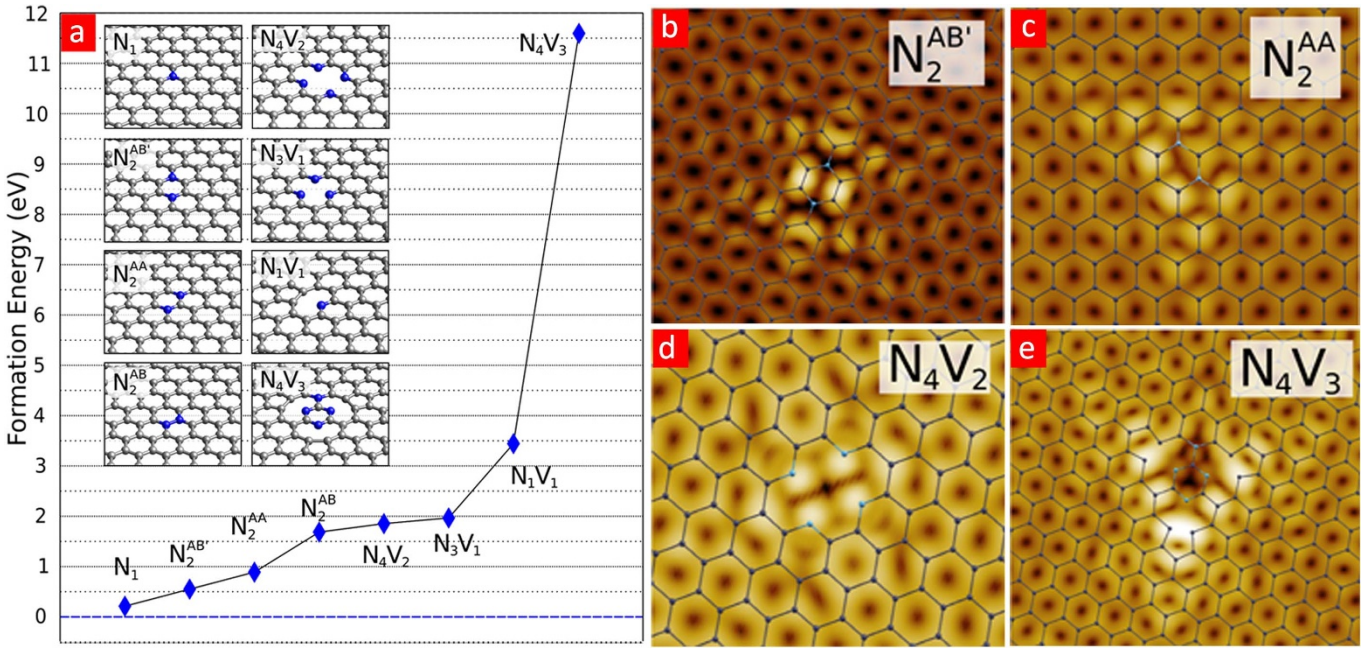

Figure 4 | Calculated formation energy, experimental and simulated STM images of different N-doping configurations. (a) Formation energies of different N-doping configurations in NG sheets (as illustrated in insets) computed using *ab initio* calculations. (b-e) Simulated STM images depicting two different atomic configurations for double substitution of nitrogen dopants (b-c) and for two pyridine-like N-dopants (d-e). The biases are as follows: (b) −1.0 eV (c) −1.0 eV (d) −0.7 eV (e) −0.7 eV. The carbon and nitrogen atoms are illustrated using gray and cyan balls, respectively. The superscript B' is used to differentiate between two N atoms as being first-nearest neighbors (N_2^{AB}) or third-nearest neighbors ($N_2^{AB'}$).

free (see Fig. S11). Only when using the appropriate temperature (800 to 850°C) and relatively long reaction times (e.g. 10 to 30 min) in the presence of NH_3, the probability of finding N_2^{AA} dopants is higher than for single N substitutions (see Fig. S9–S11). The above mechanism is also supported by STM measurements (Fig. S12). Typical STM images for NG doped at 750°C/10 min exhibits a perfect hexagonal graphene lattice without any N-dopant. For the sample doped at 800°C/30 min, STM image shows the highly crystalline graphene lattices and the presence of some N-dopants. This sample contains both N_2^{AA} and single-substitutional N dopants. The N-doping concentration using STM images is estimated to be *ca.* 2.5×10^{12} N atoms per cm^2.

By counting the density of dopants in the optimized conditions (e.g. NH_3 flow for 10 min at 850°C), and considering the fact that the abundant N_2^{AA} dopant includes two nitrogen atoms, the N-doping concentration is estimated to be *ca.* 0.25 at%, which corresponds to 5×10^{12} N_2^{AA} dopants per cm^2. Although this value only gives the local concentration within the scanned area, it is in the same order of our estimation (1.2×10^{12} cm^{-2}) from Raman measurements by considering the statistical error. As mentioned above, our STM observations suggest that most of the nitrogen incorporation occurs in the same sub-lattice (N_2^{AA}). Such a doping unbalance between two sublattices of NG could have a strong impact on its electronic transport properties, and further theoretical and experimental works on this direction are currently in progress.

The presence of N-dopants leads to significant changes in the local density of states (LDOS), which were systematically measured by differential conductance *dI/dV* spectroscopy using the lock-in technique. Spectra collected far away from the N atoms represent the unperturbed electronic structure of pristine graphene (see the olive dot curve in Fig. 5a). In order to avoid confusions, we labeled it as "undoped region". A typical V-shaped curve with a depression near the Fermi level is observed, which reveals the presence of phonon-assisted inelastic tunneling, as previously reported for monolayer graphene[39]. In comparison, the *dI/dV* spectrum near a N_2^{AA} dopant (see red curve in Fig. 5a) exhibits an enhancement in the LDOS at around +0.2 eV as well as a larger electron-hole asymmetry, caused by the presence of N atoms within the graphene lattice. It should be noted that the STS of the "undoped region" in as-synthesized NG samples is different when compared to a pristine graphene film synthesized using similar parameters (see Fig. S13). STS of pristine graphene clearly shows the Dirac point at about +0.3 V, while in our NG case, the Dirac point is located at about −0.18 V. Therefore, it could be concluded that the introduction of nitrogen atoms into graphene results in an *n*-type doping of the sample.

Our STM observations revealed that most of the N-doping sites (more than 80%) in our samples follow the N_2^{AA} configuration and they are arranged randomly within the scanning region. It is noteworthy that the N_2^{AA} defect contains three coordinated nitrogen atoms and its abundance is also consistent with XPS data (see Fig. 2d) indicating that most of the N-C bonds are three coordinated (substitutional-type nitrogen given by the N1s signal centered at *ca.* 400.6 eV).

In order to obtain quantitative insight into the electronic localization around the N dopants, *dI/dV* spectra near a N_2^{AA} dopant were measured (Fig. 5b). The LDOS was estimated exactly at the center of the N_2^{AA} doping site (B point, Fig. 5b) and 5 Å away from the doping site (A and C points, Fig. 5b). The *dI/dV* spectrum at the doping site confirms the presence of high-intensity peak located at *ca.* +0.2 eV (as already illustrated in Fig. 5a). DFT calculations performed close to the scanning points (Fig. 5b) reveal projected density of states (PDOS) containing a number of resonant peaks centered *ca.* 0.4 eV above the charge neutrality point, and caused by the nitrogen p_z orbital (Fig. 5d). Since in the experiment, the Fermi energy (E_F) is

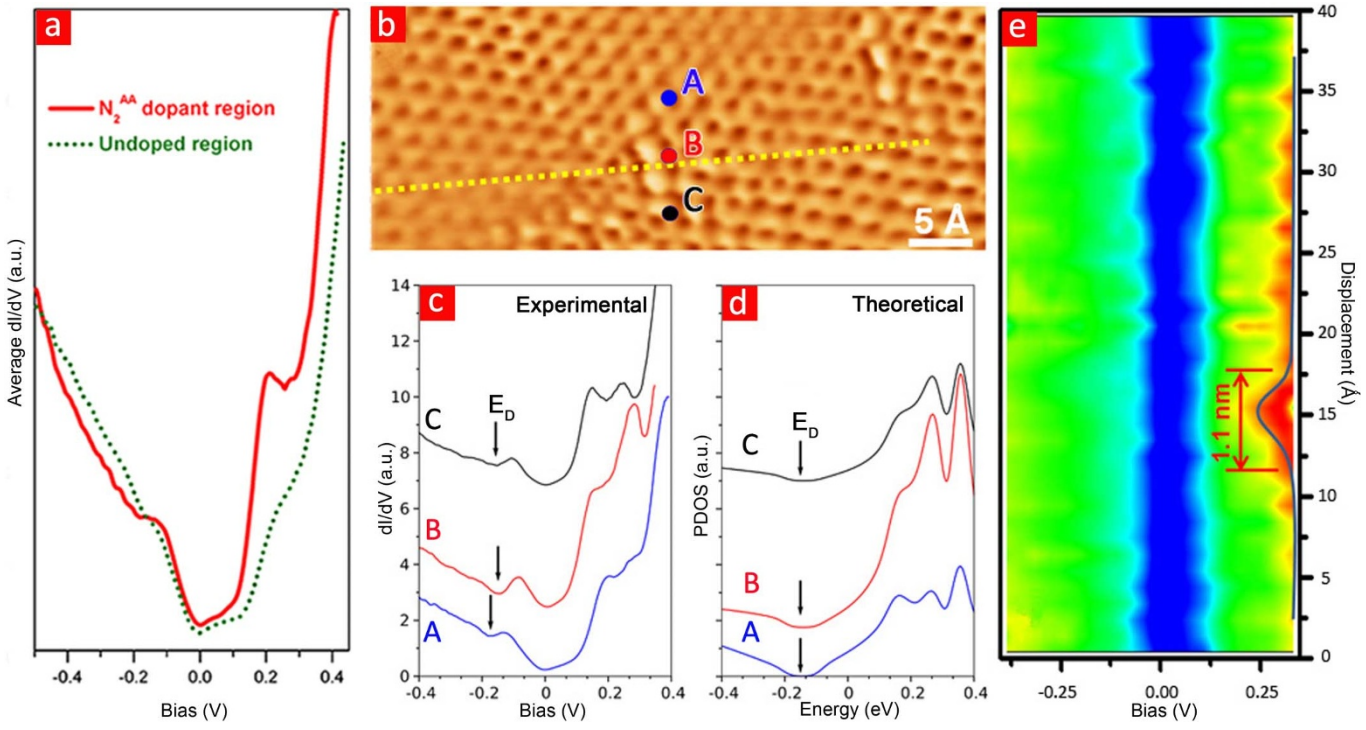

Figure 5 | Local electronic characteristics of NG sheets. (a) *dI/dV* curves measured on N_2^{AA} dopants (red solid curve) and on undoped graphene region (olive dot curve). Both *dI/dV* spectra were averaged over 9 point spectra taken in 1×1 nm^2 area. All STS data were obtained using a lock-in technique. (b) An STM topographic image including two N_2^{AA} dopants. (c) *dI/dV* curves located at the center of N_2^{AA} dopant (point B) and measured 5 Å away (points A and C). (d) Theoretical calculation of the PDOS on and near a N-dopant. The position of the Dirac point (E_D) in the calculated PDOS (d) is shifted to the experimental location for clarity. (e) A color spectra mapping across one of the dopant, as illustrated by the yellow dashed line in panel (b). The electronic perturbation induced by the N-dopant is clearly localized within ~1 nm.

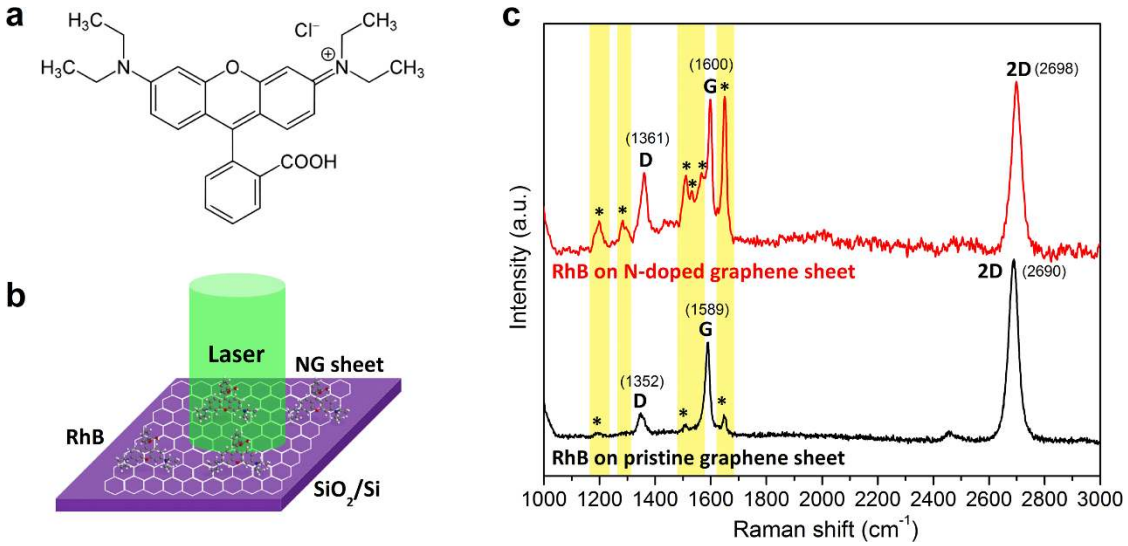

Figure 6 | Enhanced Raman scattering effect of NG sheets for probing Rhodamine B (RhB) molecules. (a) Molecular structure of RhB. (b) Schematic illustration of experimental setup. RhB molecules are anchored onto NG sheet/SiO_2/Si substrate. The laser line is 514 nm. (c) Raman signals of RhB molecules on pristine and NG sheets. The integration time is 10 s for all cases. The peaks marked with "*" are the corresponding signals from RhB molecules. Note that there is a peak of RhB at 1597 cm^{-1}, which is overlapped with the G-band of graphene sheets.

shifted from the Dirac point (E_D) due to both nitrogen and substrate doping, the Dirac point in the calculated PDOS has been aligned to the experimental position of E_D for comparison. Therefore, only the relative positions of the peaks are relevant, suggesting a good agreement between the theoretical PDOS (Fig. 5d) and the experimental STS (Fig. 5c). The PDOS on the nearest-neighbor C atom (point C) presents localized states caused by its electronic coupling with the nitrogen atom, whereas a reduced intensity of such states is observed on the next-nearest-neighbor C atom (point A). The occupied fraction of resonant states represents the localization of charge around the N-doping site. The dependence of the peak intensity with lateral displacements clearly indicates the electronic localization induced by the N dopants. Along the perpendicular direction (see dashed line in Fig. 5b), a series of dI/dV spectra were recorded across the N_2^{AA} configuration with 1Å interval. The electronic localization could be visualized by plotting the dI/dV spectra as a function of the transverse position (see color mapping in Fig. 5e). A red bump in the color map appears at positive bias, corresponding to the enhanced intensity of the resonant peaks when approaching to the N_2^{AA} dopant. By simply measuring the spatial size of the red bump, the doping effect is estimated to be localized within 1 nm. Considering a decay length of 7 Å for a single N-dopant[20], a 1 nm localization scale for the N_2^{AA} dopant constitutes a reasonable experimental value.

N-doping not only contributes to additional charge carriers and the consequent modification of graphene's electronic properties, but may also be useful in molecular sensing applications, especially the graphene-enhanced Raman scattering (GERS) of organic molecules. It has been reported that pristine graphene could result in fluorescence quenching and Raman signal enhancement of organic molecules[40,41]. The microscopic mechanism for enhanced Raman scattering on graphene substrate is still in debate, but it is suggested to follow the chemical mechanism (CM), rather than the electromagnetic mechanism (EM) observed in noble metal particles for surface enhanced Raman spectroscopy (SERS)[41]. Usually, EM is believed to be based on the enhancement of the local electromagnetic field, which is caused by the incident light-excited surface plasmons[42]. When comparing the EM with CM, it is clear that CM is based on a charge transfer established between the substrate and the probe molecules. Due to the charge transfer, the polarizability of the probe molecule will increase and thus lead to the enhancement of Raman scattering[42,43]. In our case, changes in the chemical and electronic properties of NG are expected to modify the GERS behaviour via an enhanced charge transfer. However, to the best of our knowledge, N-doped graphene has never been applied for GERS. In this study, Rhodamine B (RhB), a widely used dye (see its molecular structure in Fig. 6a), was selected as a probe molecule since it is usually very difficult to be detected by conventional Raman spectroscopy at low concentrations[44]. The presence of flat aromatic rings from RhB could closely interact with the pristine and N-doped graphene sheets so as to form a strong π-π stacking, which could contribute to a GERS enhancement[44]. Fig. 6b illustrates the GERS experimental setup for detecting RhB molecules (see Methods, Supplementary Section S8 and Fig. S14a,b for more details). Due to the strong fluorescence signal arising from the molecule, no clear Raman peaks from RhB molecules could be observed from the Raman spectra when using a bare SiO_2/Si wafer as substrate (Fig. S14c). As expected, pristine (undoped) graphene sheets successfully quench the fluorescence background and the spectrum exhibits vibrational peaks that correspond to some of the Raman fingerprints of RhB molecules at 1198 cm^{-1}, 1511 cm^{-1} and 1650 cm^{-1} (see peaks with "*" marks in Fig. 6c). Interestingly, when NG sheet is used as a substrate, the intensities of all the Raman peaks associated to RhB are remarkably improved and clearly resolved. Furthermore, additional vibration fingerprints of RhB molecules located at 1282 cm^{-1}, 1531 cm^{-1} and 1567 cm^{-1} which are not observed when using undoped graphene as a substrate, could be clearly detected. It is noteworthy that the intensity of the peak located at 1650 cm^{-1} for RhB on NG sheets is 10 times stronger than that on pristine graphene. Therefore, NG could be considered as an excellent substrate for a unique type of molecular sensing. The GERS effect has been observed when fine tuning the Fermi level of graphene by changing the electrostatic potential in a back-gated device[45]. In our case, the tuning of the Fermi level is achieved chemically through nitrogen doping. As mentioned above, the GERS enhancement of organic molecules on graphene sheets can be usually attributed to the charge transfer between molecules and the graphene surfaces[45], which could possibly lead to a molecular *p*-doping of NG in the present case. This fact could also be clearly witnessed from the remarkable upshift of the corresponding Raman peaks (D-, G- and 2D-bands) of NG sheets when they are in contact with RhB molecules (see Supplementary Fig. S15 and Table S1). Therefore, we expect that other similar acceptor-

type molecules (similar to RhB) could be efficiently detected using NG, and this unique property should be exploited in the near future and studied in more detail.

In summary, we have successfully synthesized NG via a simple and efficient AP-CVD method, and demonstrated that the introduction of nitrogen atoms within the same graphene sub-lattice could significantly alter its local electronic and chemical properties. New types of doping configurations, such as double-substitution of nitrogen (N_2^{AA}), have been confirmed experimentally and theoretically. The abundance of the N_2^{AA} doping configuration appears to be observed selectively in NG samples obtained by the synthesis method reported here. Moreover, a novel and outstanding Raman enhancement of RhB molecules was demonstrated when using NG sheet as a substrate. These findings support the idea that chemical doping with heteroatoms, such as N, B or P, could be further exploited to tailor the electronic and chemical properties of graphene, and eventually lead to selective and efficient molecular sensors. In addition, we believe that our method could be exploited further in order to specifically control the type of N-doping configurations, and their location within the two different graphene sub-lattices, thus leading to a wide variety of sheets with different physico-chemical properties that could be used as components in different electronic and sensing devices.

Methods

Synthesis of NG sheets. The growth of NG sheets was achieved in an AP-CVD system, as illustrated in Fig. S1. More details could be found in Supplementary Section S1. A typical run for NG synthesis can be described as follows. Firstly, copper foils (99.8% purity, 25 μm thick, Alfa Aesar) were cleaned in a diluted HCl aqueous solution and then placed in the center of the AP-CVD reactor. Before heating the reactor up, a mixture of Ar (1000 sccm) and H_2 (50 sccm) was introduced into the reactor to degas the air inside. Subsequently, the reactor was heated up to 980°C at a rate of 20°C/min, and kept constant for 10 min in order to anneal the copper foils. After that, CH_4 (10 sccm) was fed into the reactor at 980°C for 30 min. After that, the feeding of CH_4 was cut off and the reactor was cooled down to 850°C. Then, NH_3 (5.0 sccm) was introduced into the reactor for 10 min at 850°C. Finally, the reactor was cooled down to room temperature in an Ar flow. By using $FeCl_3$/HCl (0.5 M/0.5 M) mixture as a copper etchant (see Supplementary Section S2 and Fig. S2–S3), large-area NG sheets could be easily transferred from copper foils to other substrates (SiO_2/Si wafer, TEM grid) for further characterizations (Raman spectroscopy, XPS, STM/STS and HRTEM).

STM measurements. STM measurements were conducted with a home-built variable temperature STM in an ultrahigh vacuum (UHV) system with a base pressure better than 1×10^{-10} mbar. The NG/SiO_2/Si samples were loaded into the low-temperature STM. The samples were degassed in UHV at 200~300°C for several hours before performing the STM/STS measurements. In this study, all the STM/STS data were acquired at 85 K if not otherwise stated. A commercial Pt-Ir tip was prepared by gentle field emission at a clean Au(111) sample. The bias voltage was applied on the sample during the STM observations. The STM images were analyzed using WSxM (30).

Raman spectroscopy and mapping. Raman measurements were performed by a Renishaw inVia confocal micro-Raman spectrometer with a 100× objective and 514 nm laser as excitation source. For Raman mapping, the sample was placed on an *x-y* piezo-motorized stage and raster scanned with a step size of 400 nm for both *x* and *y* directions.

Theoretical simulations of different doping configurations. STM simulations were carried out within the Tersoff-Hamann approach-based density functional theory (DFT) by using a localized numerical basis set and norm-conserving pseudopotentials as implemented in the SIESTA package[46]. *ab initio* DFT calculations were performed using the generalized gradient approximation (GGA)[38] for the exchange correlation functional using norm conserving pseudo-potentials[47] and a numerical localized combination of atomic orbitals to expand the wave-functions. The energy levels are populated using a Fermi-Dirac distribution with an electronic temperature of 250 K and an energy cutoff of 500 Ry is used. The integration over the 2D Brillouin zone is replaced by a summation over a Monkhorst-Pack (MP) grid of 8×8 k-points. The total and partial density of states were plotted using an interpolated 24×24 MP k-point grid, and smeared with Gaussian functions with a spread of 0.03 eV. The geometries are fully relaxed until the forces on each atom and stress tolerance are less than 0.01 eV/Å and 0.01 GPa, respectively. STM images were simulated using the Tersoff-Hamman approach, by integrating the local density of states within an energy window chosen to be close to the experimental bias. For the computation of the formation energies, a correction for the basis set superposition error was included when needed.

GERS measurement. Rhodamine B (Alfa-Aesar) was used as the probe molecule. The pristine and N-doped graphene sheets on SiO_2/Si wafers were incubated in a RhB/ethanol solution with a concentration of 5×10^{-5} mol/L for 10 min (Fig. S14a). After that, the samples were rinsed with ethanol to remove the unadsorbed molecules and then dried under an argon gas flow. GERS spectra were recorded using a Renishaw inVia confocal micro-Raman spectrometer with a 100× objective. The laser spot size is less than 1 μm. The GERS measurement was illustrated in Fig. S14b. For all cases, the laser line and integration time are 514 nm and 10 s, respectively.

1. Charlier, J. C. *et al.* Enhanced electron field emission in B-doped carbon nanotubes. *Nano Lett.* **2**, 1191–1195 (2002).
2. Terrones, M. *et al.* N-doping and coalescence of carbon nanotubes: synthesis and electronic properties. *Appl. Phys. A-Mater. Sci. Process.* **74**, 355–361 (2002).
3. Villalpando-Paez, F. *et al.* Fabrication of vapor and gas sensors using films of aligned CNx nanotubes. *Chem. Phys. Lett.* **386**, 137–143 (2004).
4. Cruz-Silva, E., Barnett, Z. M., Sumpter, B. G. & Meunier, V. Structural, magnetic, and transport properties of substitutionally doped graphene nanoribbons from first principles. *Phys. Rev. B* **83**, 155445 (2011).
5. Panchokarla, L. S. *et al.* Synthesis, structure, and properties of boron- and nitrogen-doped graphene. *Adv. Mater.* **21**, 4726–4730 (2009).
6. Wang, X. R. *et al.* N-doping of graphene through electrothermal reactions with ammonia. *Science* **324**, 768–771 (2009).
7. Dai, J. Y., Yuan, J. M. & Giannozzi, P. Gas adsorption on graphene doped with B, N, Al, and S: A theoretical study. *Appl. Phys. Lett.* **95**, 232105 (2009).
8. Zou, Y. *et al.* An ab initio study on gas sensing properties of graphene and Si-doped graphene. *Eur. Phys. J. B* **81**, 475–479 (2011).
9. Meyer, J. C. *et al.* Experimental analysis of charge redistribution due to chemical bonding by high-resolution transmission electron microscopy. *Nat. Mater.* **10**, 209–215 (2011).
10. Cui, T. X. *et al.* Synthesis of nitrogen-doped carbon thin films and their applications in solar cells. *Carbon* **49**, 5022–5028 (2011).
11. Lv, R. T. *et al.* Open-ended, N-doped carbon nanotube-graphene hybrid nanostructures as high-performance catalyst support. *Adv. Funct. Mater.* **21**, 999–1006 (2011).
12. Qu, L. T., Liu, Y., Baek, J. B. & Dai, L. M. Nitrogen-doped graphene as efficient metal-free electrocatalyst for oxygen reduction in fuel cells. *ACS Nano* **4**, 1321–1326 (2010).
13. Elias, A. L. *et al.* Viability studies of pure carbon- and nitrogen-doped nanotubes with Entamoeba histolytica: From amoebicidal to biocompatible structures. *Small* **3**, 1723–1729 (2007).
14. Carrero-Sanchez, J. C. *et al.* Biocompatibility and toxicological studies of carbon nanotubes doped with nitrogen. *Nano Lett.* **6**, 1609–1616 (2006).
15. Wang, Y., Shao, Y. Y., Matson, D. W., Li, J. H. & Lin, Y. H. Nitrogen-doped graphene and its application in electrochemical biosensing. *ACS Nano* **4**, 1790–1798 (2010).
16. Wei, D. C. *et al.* Synthesis of N-doped graphene by chemical vapor deposition and its electrical properties. *Nano Lett.* **9**, 1752–1758 (2009).
17. Sun, Z. Z. *et al.* Growth of graphene from solid carbon sources. *Nature* **468**, 549–552 (2010).
18. Jin, Z., Yao, J., Kittrell, C. & Tour, J. M. Large-scale growth and characterizations of nitrogen-doped monolayer graphene sheets. *ACS Nano* **5**, 4112–4117 (2011).
19. Zhao, L. Y. *et al.* Visualizing individual nitrogen dopants in monolayer graphene. *Science* **333**, 999–1003 (2011).
20. Deng, D. H. *et al.* Toward N-doped graphene via solvothermal synthesis. *Chem. Mater.* **23**, 1188–1193 (2011).
21. Reina, A. *et al.* Large Area, Few-Layer Graphene Films on Arbitrary Substrates by Chemical Vapor Deposition. *Nano Lett.* **9**, 30–35 (2009).
22. Regan, W. *et al.* A direct transfer of layer-area graphene. *Appl. Phys. Lett.* **96**, 113102 (2010).
23. Ferrari, A. C. *et al.* Raman spectrum of graphene and graphene layers. *Phys. Rev. Lett.* **97**, 187401 (2006).
24. Yu, Q. K. *et al.* Control and characterization of individual grains and grain boundaries in graphene grown by chemical vapour deposition. *Nat. Mater.* **10**, 443–449 (2011).
25. Lucchese, M. M. *et al.* Quantifying ion-induced defects and Raman relaxation length in graphene. *Carbon* **48**, 1592–1597 (2010).
26. Jorio, A. *et al.* Measuring disorder in graphene with the G and D bands. *Physica Status Solidi B-Basic Solid State Physics* **247**, 2980–2982 (2010).
27. Dresselhaus, M. S., Dresselhaus, G. & Hofmann, M. Raman spectroscopy as a probe of graphene and carbon nanotubes. *Philosophical Transactions of the Royal Society a-Mathematical Physical and Engineering Sciences* **366**, 231–236 (2008).
28. Reddy, A. L. M. *et al.* Synthesis of nitrogen-doped graphene films for lithium battery application. *ACS Nano* **4**, 6337–6342 (2010).
29. Das, A. *et al.* Monitoring dopants by Raman scattering in an electrochemically top-gated graphene transistor. *Nat. Nanotechnol.* **3**, 210–215 (2008).
30. Elias, A. L. *et al.* Spectroscopic Characterization of N-Doped Single-Walled Carbon Nanotube Strands: An X-ray Photoelectron Spectroscopy and Raman Study. *J. Nanosci. Nanotechnol.* **10**, 3959–3964 (2010).
31. Giovannetti, G. *et al.* Doping graphene with metal contacts. *Phys. Rev. Lett.* **101**, 026803 (2008).

32. Khomyakov, P. A. *et al*. First-principles study of the interaction and charge transfer between graphene and metals. *Phys. Rev. B* **79**, 195425 (2009).
33. Rutter, G. M. *et al*. Scattering and interference in epitaxial graphene. *Science* **317**, 219–222 (2007).
34. Cockayne, E. *et al*. Grain boundary loops in graphene. *Phys. Rev. B* **83**, 195425 (2011).
35. Hohenberg, P. & Kohn, W. Inhomogeneous Electron Gas. *Phys. Rev. B* **136**, B864–871 (1964).
36. Kohn, W. & Sham, L. J. Self-consistent equations including exchange and correlation effects. *Phys. Rev.* **140**, 1133–1138 (1965).
37. Tersoff, J. & Hamann, D. R. Theory of the scanning tunneling microscope. *Phys. Rev. B* **31**, 805–813 (1985).
38. Perdew, J. P., Burke, K. & Ernzerhof, M. Generalized gradient approximation made simple. *Phys. Rev. Lett.* **77**, 3865–3868 (1996).
39. Zhang, Y. B. *et al*. Giant phonon-induced conductance in scanning tunnelling spectroscopy of gate-tunable graphene. *Nat. Phys.* **4**, 627–630 (2008).
40. Xie, L. M., Ling, X., Fang, Y., Zhang, J. & Liu, Z. F. Graphene as a Substrate To Suppress Fluorescence in Resonance Raman Spectroscopy. *J. Am. Chem. Soc.* **131**, 9890–9891 (2009).
41. Ling, X. *et al*. Can graphene be used as a substrate for Raman enhancement. *Nano Lett.* **10**, 553–561 (2010).
42. Otto, A., Mrozek, I., Grabhorn, H. & Akemann, W. Surface-enhanced Raman scattering. *J. Phys.-Condes. Matter* **4**, 1143–1212 (1992).
43. Persson, B. N. J., Zhao, K. & Zhang, Z. Y. Chemical contribution to surface-enhanced Raman scattering. *Phys. Rev. Lett.* **96**, 207401 (2006).
44. Yu, X. X. *et al*. Tuning chemical enhancement of SERS by controlling the chemical reduction of graphene oxide nanosheets. *ACS Nano* **5**, 952–958 (2011).
45. Xu, H., Xie, L. M., Zhang, H. L. & Zhang, J. Effect of graphene Fermi level on the Raman scattering intensity of molecules on graphene. *ACS Nano* **5**, 5338–5344 (2011).
46. Soler, J. M. *et al*. The SIESTA method for ab initio order-N materials simulation. *J. Phys.-Condes. Matter* **14**, 2745–2779 (2002).
47. Troullier, N. & Martins, J. L. Efficient pseudopotentials for plane-wave calculations. *Phys. Rev. B* **43**, 1993–2006 (1991).

Acknowledgments

M.T. and J.Z. thank the Penn State Center for Nanoscale Science for a seed grant entitled 'Defect Engineering of 2-D Sheets of Layered Materials'. M.T. also acknowledges the support from the Research Center for Exotic Nanocarbons, Japan regional Innovation Strategy Program by the Excellence, JST. A.R.B.M. acknowledges support from the *M. de Merre* prize of Louvain. The STM research was conducted at the Center for Nanophase Materials Sciences (CNMS), which is sponsored at Oak Ridge National Laboratory by the Scientific User Facilities Division, Office of Basic Energy Sciences, U. S. Department of Energy. This research is directly connected to the F.R.S.-FNRS of Belgium, the Belgian Program on Interuniversity Attraction Poles and to the ARC on « Graphene StressTronics » sponsored by the Communauté Française de Belgique. M.T. and R.T.L. thank T. Fujimori and F. López-Urías for fruitful discussions about GERS experiments and growth mechanism, respectively. We also thank S. Feng and S. A. Rosas for their contributions in carrying out some of the control experiments. Computational resources were provided by the CISM of the Université catholique de Louvain (GREEN and LEMAITRE computers). H.T. acknowledges funding from Programa Professor Visitante do Exterior - PVE as "Bolsista CAPES/BRASIL". The authors acknowledge the Materials Research Institute at Penn State for the use of characterization facilities.

Author contributions

M.T. and R.T.L. conceived the project. R.T.L. and H.R.G. designed and assembled the atmospheric-pressure CVD setup. R.T.L. optimized the experimental parameters and synthesized NG sheets. R.T.L. transferred the NG sheets from copper foils to other substrates (e.g. silicon wafer, TEM grid). T.H., Y.A.K and H.M. performed HRTEM measurements. A.B. performed the Raman mapping measurements. B.W. carried out the AFM measurement. R.T.L., A.L.E. and R.C.S. did the XPS measurements and analysis. A.R.B.M. and R.T.L. carried out the control experiments and Raman statistical analysis. Q.L. and M.H.P. performed the STM measurements and analysis. A.R.B.M. and J.C.C. performed the theoretical calculations and STM simulations. R.T.L. and Q.Z.H. carried out the graphene-enhanced Raman scattering (GERS) experiments and data analysis. J.Z., M.E. and H.T. discussed the results and gave constructive advices on this work. R.T.L., Q.L., A.R.B.M., J.C.C., M.H.P. and M.T. wrote the manuscript. All authors commented the manuscript.

Additional information

Supplementary information accompanies this paper at http://www.nature.com/scientificreports

Competing financial interests: The authors declare no competing financial interests.

License: This work is licensed under a Creative Commons Attribution-NonCommercial-NoDerivative Works 3.0 Unported License. To view a copy of this license, visit http://creativecommons.org/licenses/by-nc-nd/3.0/

How to cite this article: Lv, R. *et al*. Nitrogen-doped graphene: beyond single substitution and enhanced molecular sensing. *Sci. Rep.* **2**, 586; DOI:10.1038/srep00586 (2012).